

## IMAGE RANGING SYSTEM FOR UNDERWATER APPLICATIONS

Josep Forest, Joaquim Salvi, Joan Batlle

*Institut d'Informàtica i Aplicacions  
Universitat de Girona  
Lluís Santaló S/N 17071 Girona -Catalonia-  
e-mail: forest@eia.udg.es*

**Abstract:** This paper presents a computer vision and a slit laser beam which have been integrated in order to build up a fully operative 3D vision measurement system. The paper explains the laser modelling, the extrinsic and intrinsic camera calibration using a linear model, and some experimental results of 3D reconstruction. A method for automatically calibrating the laser system with few restrictions of position and orientation with respect to the camera is explained in detail. This system has been developed to improve the autonomy of the ROV GARBÍ, increasing its computer vision capabilities, incorporating 3D sensing features. Moreover, this paper addresses the constraints related to underwater imaging by using such a sensor, i.e. swaying and drifting of the vehicle due to marine currents or turbulences, water scattering and high light attenuation. *Copyright © 2000 IFAC.*

**Keywords:** Underwater Imaging, Calibration, Laser, 3D Information, Scattering.

### 1. INTRODUCTION

In the last few years, the development of AUVs has experienced a great upsurge. There is no doubt that there's a lot of interest in developing robots to carry out the unpleasant and dangerous underwater tasks which, nowadays, are done by humans. With this idea in mind, most of the efforts are focused on visual servoing, that is, on self-positioning the robot with respect to an object by using computer vision. It is well-known that underwater visual servoing becomes more difficult in unstable sea movement. The task of grabbing proper images under such circumstances is the primary problem which has to be solved in order to carry out complicated tasks such as object manipulation. Some research has been done with the aim of doting the Vortex underwater vehicle by a visual sensor based on the projection of a laser beam slit (Coste-Manière *et al.* 1996). This sensor has been used in underwater pipe inspection (Rives and Borrelly 1997). However,

the main problem of single slit projection is the reduced area which can be analysed. Of course, this problem can be solved by acquiring more scene information by the projection of more than a single slit, forming a stripped or grid pattern (Jarvis 1983). However, the correspondence problem between captured and projected slits has then to be taken into account (Ridao *et al.* 1998). Our approach is based on using a scanning laser slit. Using this approach the problem of correspondence is overcome by considering one slit projection at a time among a set of projections over time. In this way, time and the fact that there can't be more than one line on the same row of the image identifies each pixel uniquely.

The use of acoustic active systems has not been considered due to their slow acquisition rates and lack of accuracy compared to the thickness of a laser line. Acoustic imaging is very useful when building surface maps of the bottom because a simple cheap device can be mounted under a ship's



Fig. 1. GARBI: A low cost underwater robot.

keel. Map building is achieved by ordering the ship a straight rhumb.

Acoustic systems are not suitable for reconstruction of moving objects. Furthermore, static bottom-locked acoustic devices are very useful for position detection of *any thing* within a determined area, but they are useless if we are intending to build a system that can be carried by the robot itself in order to be positioned with respect to any natural element such as rocks or wall prominences or even man made elements such as the mast of an immersed ship.

The presented sensor will be mounted on our ROV called GARBI. GARBI (figure 1) is a project financed by the Spanish government<sup>1</sup> and jointly developed between the Polytechnical University of Catalonia and the University of Girona. The robot has been primarily used in tele-operated tasks like underwater inspection (Amat *et al.* 1995). It has also been used in underwater object manipulation by using its two tele-manipulated arms.

This paper is structured as follows. Firstly, the underwater robot is briefly introduced. Then, the camera and laser beam modelling and calibrating is explained in section 3. Section 4 includes the principle used to reconstruct the scene. Section 5 shows the experimental results. The paper ends with conclusions and further work.

## 2. THE UNDERWATER ROBOT

The vehicle developed was conceived for exploration in waters up to 200 meters. The robot has 4 degrees of freedom, corresponding to the linear movements of advancing, descending, turning, and pitching. These movements are achieved by 4 propellers. With the aim of building a low cost

underwater vehicle, GARBI was constructed using low cost materials, such as fibre-glass and epoxy resins. To solve the problem of resistance to underwater pressure, the vehicle is servo-pressurised to the external pressure using a compressed air bottle like those used in SCUBA diving. Air consumption is required only in vertical displacements during which the decompression valves release the required amount of air to maintain the internal pressure at the same level as the external one. The vehicle is equipped with two arms, thus it can, through tele-operation, perform some tasks of object manipulation (Amat *et al.* 1995). The robot interior has been organised so as to install the following equipment: (1) Laser beam projecting system, (2) RGB Camera, (3) PC computer, (4) Power interface for the thrusters and arm motors and (5) Batteries.

## 3. THE USE OF LIGHT UNDERWATER: SCATTERING AND ABSORPTION

The use of light in underwater environments is subject to the consideration of physical phenomena such as scattering and absorption, both of them present in the surface too, but considered only when very long distances or dusty environments are involved for measurement purposes in free air.

An exhaustive thorough study of light scattering by particles can be found in (Van de Hulst 1981).

Scattering becomes a major factor in underwater illumination systems due to the large amount of particles present within the water. This phenomena causes a change in light Intensity, Polarisation and Phase, although the loss of intensity is the most relevant drawback to be taken into account, due to the limitation it imposes to the distance the light can achieve. Scattering is the fact that light is reflected on the multiple floating particles within the water. Scattering can be observed too in free air when light passes through the mist or a cloud. Figure shows scattered light due to a particle is characterized by the scattering angle  $\theta$ .

Absorption of light is a relevant aspect as well. It is much more important underwater than in free air for the same reason than scattering. Absorption takes place when part of the incident light is absorbed by a particle. This absorbed light, that can be thought of as energy, is transformed to some other form of energy (heat, for example), so the remaining light has less intensity than the incident one.

The combination of both scattering and absorption phenomena makes the light suffer an Extinction, which is the total absence of a particular wavelength at a determined distance from the

<sup>1</sup> CICYT Program, No TAP92-0792, 1992/1994; TAP95-0426-C02-02, 1994/1996; MAR97-0925-C02-02, 1997/1999

focus of light. As it is stated in (Van de Hulst 1981):

Extinction = scattering + absorption.

In order to avoid an early extinction of the light, more powerful light sources should be used, as well as choosing a coherent light source (laser) centered at a proper wavelength. Red is rapidly extinguished with distance underwater, but blue is the later wavelength to disappear. In our system, a green ( $400\text{nm} < \lambda < 710\text{nm}$ , 5mW output power) semiconductor laser has been chosen as a compromise between extinction and cost effectiveness.

#### 4. THE RANGE IMAGING SYSTEM

The laser beam rotates by means of a DC motor in order to scan the whole camera scope getting a reconstruction of the front scene. A green laser beam was chosen because it is less affected by scattering than a red one, thus enlarging the camera scope and facilitating accurate segmentation results under no light control scenarios. The power control card was adapted to the new drivers technology and integrates the supply, the motor PWM control and the incremental encoder used to obtain the angular position of the laser beam. Furthermore, a processing card was used in order to segment the image and obtain the 2D co-ordinates of the laser beam in the image plane at video rate. The processing card converts the space colour from RGB to HLS and segments the laser light from the rest of the scene by using LUT memories (Batlle 1993). Thereafter, the card processes the video lines with the aim of obtaining the 2D co-ordinates. The first co-ordinate is given by the video line explored by the card, the second co-ordinate is given by computing the gravity centre of the segmented pixels. The card also synchronises the camera with the laser and gets the angular position of it for each image shot. Once the whole image has been processed the information is sent to the computer which produces the 3D reconstruction.

##### 4.1 Camera Modelling and Calibration

The pinhole model is based on reducing the complexity of camera behaviour to an image plane  $\Pi$  where the scene is projected through the focal point  $O_c$  (Fangeras 1993). The focal point is then placed at a fixed distance  $f$  from the image plane eliminating lens distortion. Then, giving a 3D object point  $P$  its 2D image projection  $p$  is obtained by the intersection of the optical ray  $v$  defined by  $P$  and  $O_c$  and the image plane  $\Pi$ . This model is defined by two transformation matrices  ${}^cT_W$  and  ${}^lT_C$ .  ${}^cT_W$  deals with the extrinsic parameters which express the position and orientation of

the world co-ordinate system  $\{W\}$  with respect to the camera co-ordinate system  $\{C\}$ .  ${}^lT_C$  models the intrinsic parameters which express the optical characteristics and internal geometry of the camera. That is, the projection of the focal point  $O_c$  on the image plane  $(u_0, v_0)$  and the  $(\alpha_u, \alpha_v)$  parameters which permit the transformation from the camera co-ordinate system in millimetres to the image co-ordinate system in pixels.

The camera model determines the relationship between the 3D object point  $P$  and its 2D image point projection  $p$  by using the equation (1).

$$\begin{bmatrix} s^l X_i \\ s^l Y_i \\ s \end{bmatrix} = {}^lT_C {}^cT_W \begin{bmatrix} w X_i \\ w Y_i \\ w Z_i \\ 1 \end{bmatrix} \quad (1)$$

$$\text{where } {}^cT_W = \begin{bmatrix} R_{3 \times 3} & t_{3 \times 1} \\ 0_{1 \times 3} & 1 \end{bmatrix}$$

$$\text{and } {}^lT_C = \begin{bmatrix} \alpha_u & 0 & u_0 \\ 0 & \alpha_v & v_0 \\ 0 & 0 & 1 \end{bmatrix}$$

Camera calibration is based on obtaining the intrinsic and extrinsic parameters of the camera model from a set of 3D object points with respect to the world co-ordinate system and their 2D image points with respect to the image co-ordinate system. The  $n$  3D object points are obtained by using a calibrating pattern in which the 3D components can be easily measured. The 2D image points are obtained by measuring the projection of the 3D object points on the image plane of the camera. By using the equation (1) and arranging the unknowns the equation (2) is obtained, in which  $B$  is a vector of  $2n$  components which contain the 2D image point components.  $Q$  is a matrix of  $2n$  rows and 10 columns expressing the relationship between 2D and 3D points; and  $X$  is the vector of the 10 camera model unknowns which can be obtained by using the equation (3) (Salvi 1997).

$$B = QX \quad (2)$$

$$X = (Q^T Q)^{-1} Q^T B \quad (3)$$

The more points we use to calibrate the camera the more accuracy is obtained. However, we also have to take care with the accurate measurement of the 3D object points of the calibrating pattern and their 2D image point projections.

##### 4.2 Laser Model and Calibration

In order to get accurate reconstructions of the scene, the laser geometry (shape, position and orientation) with respect to a reference coordinate

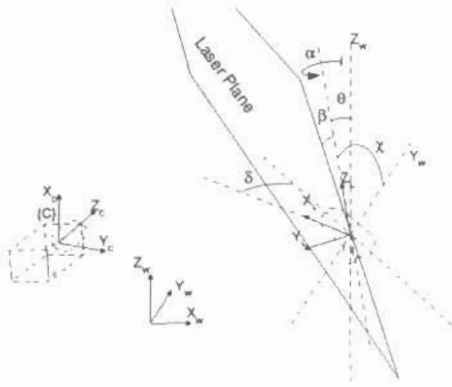


Fig. 2. Laser system with the 8 parameters describing its model.

system  $\{W\}$  must be known. To this aim, the system has been modeled as shown in figure 2. In this model no constraints in the position, orientation or movement of the laser with respect to  $\{W\}$  have been considered. The laser slit has been considered as a plane which rotates around the  $Z_L$  axis of the laser coordinate system  $\{L\}$ .

Within these considerations, up to 8 parameters have to be considered:

- $X$ ,  $Y$  and  $Z$  determine the position of the laser coordinate system  $\{L\}$  with respect to the reference coordinate system  $\{W\}$ .
- $\alpha$  is the angle of rotation around  $Z_L$ , measured from  $X_L$ , while  $\delta$  is the offset angle of rotation of  $\{L\}$  with respect to  $Z_L$ , due to the mechanical misalignment between  $X_L$  and the mechanical origin of the encoder.
- $\beta$  is the angle that the plane forms with  $Z_L$ , measured around  $X_L$ , due to the misalignment of the laser emitter with respect to the motor's axis of rotation.
- $\theta$  and  $\gamma$  are the pan and tilt angles of rotation of  $\{L\}$  with respect to  $X_W$  and  $Y_W$  respectively considering  $\{L\}$  and  $\{W\}$  coincide, due to errors in screwing the motor on the platform.

Among these 8 parameters, only  $\alpha$  is known in each instant of time, because it is delivered by the encoder, and is the only one that doesn't have to be found in the calibration process.

A plane in  $R^3$  is defined by a normal vector ( $\vec{v}_n$ ) and a point contained on the plane. In order to get  $\vec{v}_n$  it is first necessary to compute  ${}^W T_L$  which expresses the orientation of  $\{L\}$  with respect to  $\{W\}$ , and is achieved by considering a rotation of  $\delta$  around  $Z_W$ , followed by a rotation of  $\theta$  around  $X_W$ , and then a rotation of  $\gamma$  around  $Y_W$ .

$\vec{v}_{nL}$  (normal vector to the plane with respect to  $\{L\}$ ) is computed by a rotation of  $\beta$  around  $X_L$ ,

followed by a rotation of  $\alpha$  around  $Z_L$ , considering it is normal to the plane  $Y_L = 0$  when  $\alpha = \beta = 0$ .

In order to get  $\vec{v}_{nW}$  (the normal vector with respect to  $\{W\}$ ), it is necessary to compute  $\vec{v}_{nW} = {}^W T_L \cdot \vec{v}_{nL}$ .

Now, if we consider the restrictions  $\theta = \gamma = 0^\circ$ , for the camera and the laser system are rigidly joined, we get the final expression for  $\vec{v}_{nW}$  in equation (4).

$$\vec{v}_{nW} = \begin{bmatrix} -\sin \alpha \cos \beta \cos \delta - \cos \alpha \cos \beta \sin \delta \\ -\sin \alpha \cos \beta \sin \delta + \cos \alpha \cos \beta \cos \delta \\ -\sin \beta \\ 0 \end{bmatrix} \quad (4)$$

The laser calibration is achieved by projecting the laser slit on the calibration pattern used for calibrating the camera. Segmenting the laser colour (green) at video rate through a special purpose video pre-processing card (Batlle 1993), we get the line projection of the laser plane. After thinning the line, we have the 3D points corresponding to the laser line points. Now these points can be used in order to calibrate the laser.

As the 3D points belong to the laser plane, they can be used to get the laser plane equation  $Ax + By + Cz + D = 0$ .

Where A,B and C are the three components of the normal vector  $\vec{v}_{nW}$ , and D is defined as the dot product of a point  $P$  in the plane and  $\vec{v}_{nW}$ .

The plane equation can be operated and arranged in matrix form, obtaining equation (5).

$$\begin{bmatrix} -\sin \alpha_i & \cos \alpha_i & P_{x_i} \cos \alpha_i + P_{y_i} \sin \alpha_i & 1 \\ \vdots & \vdots & \vdots & \vdots \\ \vdots & \vdots & \vdots & \vdots \end{bmatrix} \times \begin{bmatrix} X + Y \tan \delta \\ Y - X \tan \delta \\ \tan \delta \\ \frac{\tan \beta}{\cos \delta} (P_z - Z) \end{bmatrix} = \begin{bmatrix} P_{y_i} \cos \alpha_i - P_{x_i} \sin \alpha_i \\ \vdots \\ \vdots \end{bmatrix} \quad (5)$$

As the laser can sweep over the whole calibration pattern, multiple sets of points can be obtained, so sweeping from  $\alpha = 0$  to  $\alpha = 41^\circ$ , we have one set of points corresponding to  $P_z = 0$  and another one for  $P_z = 100$ . The system can be solved by considering two sets of only 4 points, but if more points are obtained, the error due to noise in the CCD of the camera, the segmentation process or the thinning algorithm can be minimised. Using the pseudo-inverse method, the solution vector  $S$ .

$$S = \left[ X + Y \tan \delta \quad Y - X \tan \delta \quad \tan \delta \quad \frac{\tan \beta}{\cos \delta} (P_z - Z) \right]^T = [S_1 \quad S_2 \quad S_3 \quad S_4]$$

is obtained for each set of points. Using only one set of points,  $X$ ,  $Y$  and  $\delta$  can be obtained with the first 3 components of  $S$ , and using the results of  $S_4$  for the two sets, we can find a solution for  $\beta$  and  $Z$ . The expressions for  $X$ ,  $Y$ ,  $\delta$ ,  $\beta$  and  $Z$  are shown in expressions (6) to (10).

$$X = \frac{S_1 - S_2 S_3}{1 + S_3^2}; \quad (6)$$

$$Y = S_2 + X S_3; \quad (7)$$

$$\delta = \arctan(S_3); \quad (8)$$

$$\beta = \arctan\left(\frac{S_{14} - S_{24}}{(P_{x0} + P_{x100}) \cos \delta}\right); \quad (9)$$

$$Z = \frac{S_{14} \cos \delta}{\tan \beta} - P_{x0} \quad (10)$$

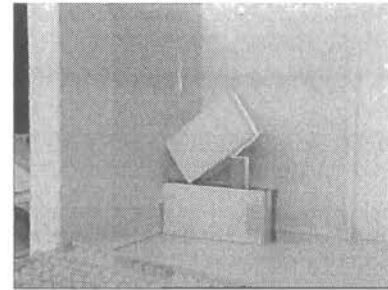
Finally, the 7 calibration parameters for the laser structure have been obtained. The procedure for obtaining them is a linear algorithm, so it is fast and more reliable as the number of 3D points increases.

## 5. EXPERIMENTAL RESULTS

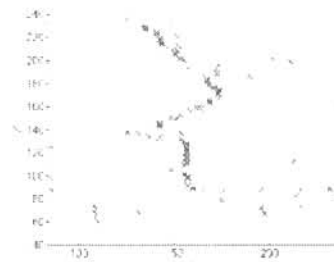
An experimental platform was built, incorporating the hardware system: camera, laser and coupling mechanisms. The camera and laser was modelled and calibrated by using two orthogonal calibrating planes with 20 equally spaced black squares on each one. The vertexes of these squares were accurately measured and used as the 3D object point set for the camera calibration. The laser system was calibrated by projecting the laser slit on both calibrating planes and measuring its 3D position, as the camera had already been calibrated. When both systems are calibrated, the system can be used for 3D reconstruction. Figure 5(a) shows the picture of the scene under test, and figure 5(b) shows its corresponding reconstruction on the plane  $YZ$  of the calibration coordinate system. The length of the slanting side of the paralelepiped is 82mm, while the reconstruction yielded a result of 79.6mm, so an error of 3% has been committed.

The laser has been tested underwater in the lake of Banyoles, in Banyoles -Catalonia-, in order to estimate how scattering influences the system's performance. In a 3 meters depth visual observations have been made in order to estimate the maximum distance from which the laser projection is clearly seen over a white screen. A distance of 2.5 meters approximately have been observed to be the maximum from where the laser becomes acceptably clear, while for bigger distances the laser projection becomes more and more fuzzy which is not desirable for an optimal color segmentation.

The system has been thought to operate accurately at 1-2 meters, otherwise the distance between the camera and the laser projector would



(a)



(b)

Picture of the scene to be reconstructed (a) and the reconstruction projection on the  $YZ$  plane (b).

be greater which is not feasible if a compact, small system has to be built. The fact that the maximum distance of clear observation is greater than the maximum distance for obtaining accurate measurements is very encouraging, mainly regarding that the water in Banyoles is quite muddy, with plenty of suspended particles within it.

As can be seen in figure 5, the whole system has not been tested in underwater scenes, only in our lab. However, the simulation results encourage us to test the system in such conditions.

## 6. CONCLUSIONS AND FURTHER WORK

We have presented a new method of calibrating a laser for a range imaging system in which up to 7 calibration parameters have been identified. This calibration method relies on the previous calibration of the camera, for which we have used a well known linear calibration method. The system can be used for 3D reconstruction of any scene and it is being tested on the underwater ROV GARBÍ.

This sensor was made with the aim of supplying 3D visual information to the control architecture of an underwater vehicle in order to implement the following behaviours: (a) **Obstacle avoidance**. The robot must avoid static and dynamic obstacles which can be found in its path, (b) **Robot stabilisation**. The robot must be stabilised and positioned keeping a constant distance and orientation with respect to an object, and (c) **Map building**. The robot wanders over the bottom of the sea or around a bounded area building a database with the 3D data.

At the time of writing, only static images have been tested, though some work is being done in order to include moving scene reconstruction capabilities, but it is still in a very early stage. In addition, a simple calibration procedure was considered to be enough for this first approach, but if more accurate results have to be obtained, the dynamic self-calibration of the system is a major topic to be considered in the future.

## 7. REFERENCES

- Amat, J., J. Codina, X. Cufi and J. Puigmal (1995). Vision based control of underwater vehicle for long duration observations. In: *Int. Conf. on Autonomous Robots*. Vol. 1. pp. 273-277.
- Batlle, J. (1993). Aportació a la detecció de moviment independentment del moviment de la càmera. PhD thesis. Universitat Politècnica de Catalunya.
- Coste-Manière, E., V. Rigaud and UNION team (1996). Union: Underwater intelligent operation and navigation. Technical Report RR-3038. INRIA.
- Faugeras, O. (1993). *Three-Dimensional Computer Vision: A Geometric Viewpoint*. The MIT Press.
- Jarvis, R. A. (1983). A perspective on range finding techniques for computer vision. *IEEE Transactions on Pattern Analysis and Machine Intelligence* 5(2), 122-139.
- Ridao, P., J. Salvi and J. Batlle (1998). Behaviours implemented using a vision system based on coded structured light projection. In: *IEE Colloquium on Underwater Applications of Image Processing*. Vol. 1998/217. pp. 7/1-7/6.
- Rives, P. and J. Borrelly (1997). Underwater pipe inspection task using visual servoing techniques. In: *IEEE/RSJ Int. Conf. on Intelligent Robots and Systems*. Vol. 1. pp. 63-68.
- Salvi, J. (1997). An Approach to Coded Structured Light to Obtain Three Dimensional Information. PhD thesis. Universitat de Girona.
- Van de Hulst, H.C. (1981). *Light Scattering by Small Particles*. Dover Publications, Inc., New York.